



Article

Effects of Ground Motion Duration on the Seismic Performance of a Two-Storey Balloon-Type CLT Building

Maral Jafari ¹, Yuxin Pan ¹, Md Shahnewaz ²  and Thomas Tannert ^{1,*} 

¹ School of Engineering, University of Northern British Columbia (UNBC), Prince George, BC V2N 4Z9, Canada; mjafari@unbc.ca (M.J.); yuxin.pan@unbc.ca (Y.P.)

² Fast + Epp, Vancouver, BC V5Y 1M2, Canada; mshahnewaz@fastepp.com

* Correspondence: thomas.tannert@unbc.ca

Abstract: The effects of long duration ground motions on the seismic performance of a newly constructed two-storey balloon-type cross-laminated timber (CLT) building located in Vancouver, Canada, was studied. A three-dimensional numerical model of the building was developed in OpenSees. The connection and shear wall models were validated with test data. Twenty-four pairs of long and short duration records with approximately the same amplitude, frequency content, and rate of energy build-up were used for nonlinear dynamic analyses. Fragility curves were developed based on the results of incremental dynamic analysis to assess the building's collapse capacity. At design intensity level, ground motion duration was shown not to be a critical factor as the difference in inter-storey drift ratio between the two sets of records was negligible. However, due to the larger number of inelastic cycles, the long duration motions increased the median probability of collapse by 9% when compared with the short duration motions. Further research is required to evaluate the duration effects on taller and platform-type CLT buildings.

Keywords: ground motion duration; cross-laminated timber; collapse capacity; dynamic analysis



Citation: Jafari, M.; Pan, Y.; Shahnewaz, M.; Tannert, T. Effects of Ground Motion Duration on the Seismic Performance of a Two-Storey Balloon-Type CLT Building. *Buildings* **2022**, *12*, 1022. <https://doi.org/10.3390/buildings12071022>

Academic Editor: Rita Bento

Received: 2 July 2022

Accepted: 13 July 2022

Published: 15 July 2022

Publisher's Note: MDPI stays neutral with regard to jurisdictional claims in published maps and institutional affiliations.



Copyright: © 2022 by the authors. Licensee MDPI, Basel, Switzerland. This article is an open access article distributed under the terms and conditions of the Creative Commons Attribution (CC BY) license (<https://creativecommons.org/licenses/by/4.0/>).

1. Introduction

1.1. Objective

Seismic activity is particularly high in the southwestern part of British Columbia (BC), Canada, with three types of earthquakes contributing to the local hazard: (i) crustal earthquakes, (ii) subduction in-slab earthquakes, and (iii) subduction interface earthquakes [1]. The latter records show exceptionally large magnitude ($M_w > 9$) and long duration (up to several minutes). Paleoseismic evidence indicates that subduction interface earthquakes occur about every 450 years in BC [2]. Since the last major subduction earthquake has been dated to more than 300 years ago [1], the subduction process in this region may cause an earthquake during the lifetime of current structures.

It has been reported that ground motion duration has an impact on structural performance, yet no study is available on cross-laminated timber (CLT) buildings. The objective of the research presented herein was to assess the effects of ground motion duration on the seismic performance of a two-storey balloon-type CLT building. The specific goals were to compute interstorey drift ratio (IDR) at various intensity levels to evaluate the building's collapse capacity under long and short duration motions. The seismic response of the building under two sets of long and short duration motions with similar amplitude, frequency content and the rate of energy build-up, was evaluated through nonlinear time history analysis (NLTHA). The collapse capacities were then identified by developing fragility curves from incremental dynamic analysis (IDA).

1.2. Effect of Ground Motion Duration on Structural Performance

Research since the early 1960s investigated the effect of ground motion duration on structural performance of steel [3–6], concrete [7–10], and light-frame wood build-

ings [11–13]. The impacts of ground motion duration were shown to depend on the material models (with or without degradation), intensity level (design or collapse), and damage measures used for assessment (e.g., drift, energy demand, or damage index).

Raghunandan and Liel [8] examined two-dimensional reinforced concrete frames of different heights and showed that IDR was not much affected by ground motion duration. However, Han et al. [9] reported that longer duration on a 4-storey reinforced concrete structure may result in larger IDR and a larger residual displacement but only for intensity levels that induce nonlinear deformation. Similarly, Barbosa et al. [5] reported that the duration effect on peak IDR of steel frame buildings is higher for larger spectral acceleration. For light-frame wood structures, Pan et al. [12] showed that long duration motions increased the probability of exceeding the design drift limit drift by 17%. Ground motion duration has also been reported to affect the collapse capacity of concrete structures [10], mid-rise wood buildings [14], steel moment frames [4,14], and reinforced concrete structures [8].

Effectively isolating duration effect from other ground-motion characteristics is a challenge. Previous research applied spectrally equivalent record pairs [14] or spectrally matched record pairs [15] to decouple the duration from amplitude and frequency content. Spectral matching eliminates spectral-amplitude differences in the ground motion records, whereas the spectrally equivalent method decouples the differences in amplitude and frequency between the record sets. These methods, however, only partially decouple the duration influence from other ground motions characteristics.

To address this challenge, Zengin et al. [4] presented a method where the rate of energy build-up of ground motions was used as a control parameter in addition to amplitude and frequency content. The rate of energy build-up in the accelerogram affects structural response, and accelerograms that quickly reach their final energy are more likely to damage and collapse structures [16]. The rate of energy build-up of ground motions can be determined by the slope of Husid plots [17], based on the rate of Arias Intensity (I_A) build-up over the significant duration. Bommer et al. [18] compared two records with an equal amount of energy but different durations indicated that the record with a steeper slope of Husid plot imposed higher energy dissipation demand.

The duration of ground motion was classified based on their 5% to 95% significant duration (D_{5-95}): the time interval between 5% and 95% of the I_A , which determines the intensity of shaking by measuring the acceleration of seismic waves [19,20]:

$$I_A = \frac{\pi}{2g} \int_0^{t_{\max}} a^2(t) dt \quad (1)$$

where $a(t)$ is the recorded ground acceleration, t_{\max} is the length of record, and g is the acceleration due to gravity. Amongst the metrics developed for measuring ground motion duration, D_{5-95} has been found to be the best indicator for evaluating the inelastic performance of structures [3].

1.3. CLT Lateral Load Resisting Systems

Due to its biaxial strength and stiffness, CLT can be used for floors and shear walls applications in lateral load resisting systems (LLRS), for both platform-type and balloon-type constructions [21–23]. In platform construction, each floor acts as a platform for the floor above, in contrast to balloon construction, where walls continue over several floors.

CLT panels are almost rigid under in-plane loading; therefore, ductility and energy dissipation in CLT shear walls must be achieved by the connections [24]. This occurs through rocking or sliding behavior. Hold-down (HDs) are designed to resist rocking and shear brackets are designed to resist sliding. Recent novel HD solutions include internal-perforated steel plates, hyperelastic bearing pads, and high-strength HDs with self-tapping screws [24].

The 2020 National Building Code of Canada (NBCC) [25] provides seismic modification factors $R_0 = 1.5$, and $R_d = 2.0$ for force-based design of CLT shear walls and refers to CSA O86 [26] for design provisions. CSA O86 specifies that energy dissipative connections

must have sufficient ductility and deformability. Non-dissipative connections must be capacity-protected to remain linear elastic under the force and displacement demands induced on them when the energy-dissipative connections reach their 95th percentile of ultimate resistance. However, these provisions apply only to platform-type construction.

The seismic performance of multi-storey platform-type CLT structures has been the subject of previous research with focus on developing design provisions, collapse capacity, drift demand, and damage measures in CLT structures. It has been reported that among different wall configurations, the panel aspect ratio is the most influential parameter affecting the wall performance [27], and that smaller wall segments connected by vertical joints are more seismically efficient [28]. The most comprehensive experimental study was the SOFIE project [29] where different CLT buildings withstood 15 consecutive destructive earthquakes without severe damage.

Balloon-type constructions receive increasing attention; Shahnewaz et al. [30] tested a two-storey balloon-type CLT shear wall with different ledgers under monotonic and cyclic loading and reported that the CSA O86 specifications for platform type construction is applicable to balloon type construction. Zhang et al. [31] investigated the effect of HD, vertical, and horizontal shear connections between the CLT panels on the period and stiffness of tall balloon-type CLT buildings and reported that the horizontal shear connections have the greatest impact on the overall stiffness of the building and this influence decreased as the building height increased.

Numerical studies have verified that component-based modelling of CLT walls using elastic shell elements and connection test data is a reasonable approach. Using IDA, Shahnewaz et al. [32] evaluated the damage states of a six-storey CLT platform-type building at various intensity levels and concluded that the building can safely be built in a high seismic zone. Sun et al. [33] determined drift limitations for mid-rise or high-rise platform-type CLT buildings, as 0.25%, 0.70%, and 1.30% for frequent, medium, and rare seismic hazard levels, respectively.

For numerical modeling of CLT LLRS, an accurate constitutive model of the connections is necessary. Some hysteretic models for simulating timber joints are available in the OpenSees platform [34]. One commonly used hysteretic model is Pinching4, which accounts for strength and stiffness degradation as well as pinching under cyclic loading. Originally was developed for the analysis of beam-column joints in reinforced concrete frame structures [35], it is now widely used for analyzing timber and steel joints.

2. Case Study Building

2.1. Building Description

The Sir Matthew Begbie Elementary School, in Vancouver BC, shown in Figure 1, was used as a case study. This two-storey school building was designed by Fast + Epp. The building consists of two blocks, north block with classrooms and south block with classrooms and a gym. This research is focused on the northern block to avoid the complexity of the southern block in the modelling. The plan dimensions for the northern building are 25.5 m by 35.1 m. Figure 2 shows the first and second floor plans of the north block. The storey heights for the first and second floor are 4.4 m and 4.0 m, respectively.

The building's gravity load resisting system consists of CLT floor panels, steel HSS columns, and CLT walls. The building's LLRS is mainly provided by two-storey continuous coupled CLT panels forming shear walls. The shear walls dissipate energy through HDs and vertical panel-to-panel joints while wall base connections (WB) were capacity protected. The seismic design of the building followed the NBCC provisions [25]. Force modification factors R_d and R_0 applied in the building are 2.0 and 1.5, respectively, which was verified through full-scale testing on balloon shear wall [30]. The soil type of the site is class C. The importance factor (I_E) for the high importance category elementary school building is 1.3.



Figure 1. Begbie elementary school (Photo courtesy of Fast + Epp).

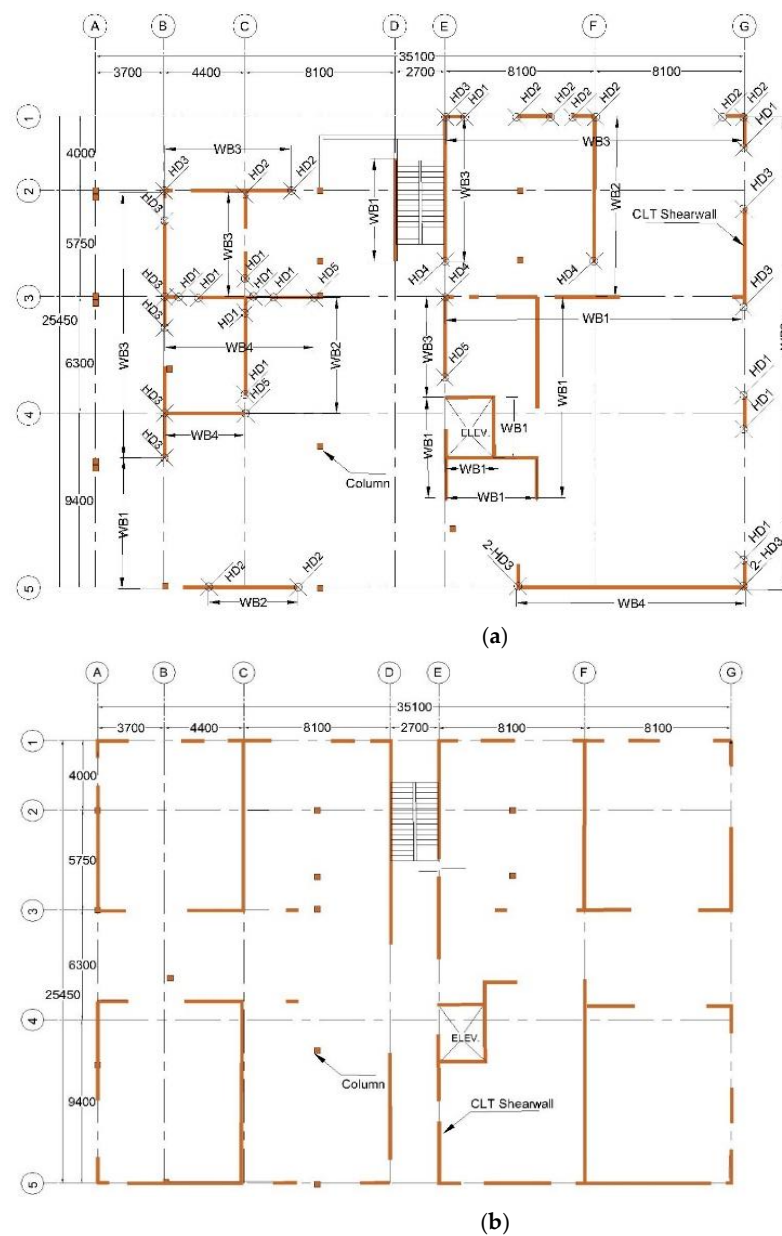


Figure 2. Plan view of northern block of building: (a) first floor, and (b) second floor (unit: mm).

For the energy dissipative connections, five types of HD connections and six types of panel-to-panel spline joints were designed. For HDs 1–3, Rothoblaas WHT angle plates with different numbers of tanker nails were used, whereas HD4/5 consists of an internal steel plate with tight-fit 12Ø pins. Plywood spline and lap spline were used for panel-to-panel joints. For the panel-to-panel vertical spline connections, surface mounted 25 mm by 140 mm D.Fir plywood pieces were attached using screws and smooth shank nails. For lap spline connections, half-lap joint connections with 80 mm lap length and maximum 2 mm gap were connected using partially threaded screws. Details on the fastener schedule are provided in Table 1.

Table 1. Connection schedule.

Mark	Type	Fasteners
HD1	WHT440	30–nails 4Ø 60 mm long.
HD2	WHT620	55–nails 4Ø 60 mm long.
HD3	WHT740	75–nails 4Ø 60 mm long.
HD4	Custom	6–12Ø stainless steel tight fit pins
HD5	Custom	10–12Ø stainless steel tight fit pins
SP1	Plywood spline	screws 8Ø 120 @ 600 mm + mails 4Ø 60 @ 250 mm
SP2	Plywood spline	screws 8Ø 120 @ 600 mm + mails 4Ø 60 @ 200 mm
SP3	Plywood spline	screws 8Ø 120 @ 600 mm + mails 4Ø 60 @ 150 mm
SP7	Half-lap joint	screws 8Ø 140 @ 250 mm–
SP8	Half-lap joint	screws 8Ø 120 @ 200 mm–
SP11	Half-lap joint with steel plate	2 rows screws 8Ø 120 @ 200 mm–

2.2. Model Development

A three-dimensional (3D) building model with six degree-of-freedom (DOF) and a two-dimensional (2D) shear wall model (for validation) with 2 DOF were developed in OpenSees, see Figure 3. Floors were modeled as rigid diaphragms with lumped mass at each story. The total seismic weights for first and second floor, including self weight of structural members, 0.5 kPa superimposed dead, and 25% snow loads are 3006 kN and 1890 kN, respectively. Floors were constrained in all DOFs except translation along X, Y, and rotation about Z axis. Supports of the building were modeled as fully fixed. The CLT walls were modeled as elastic isotropic material.

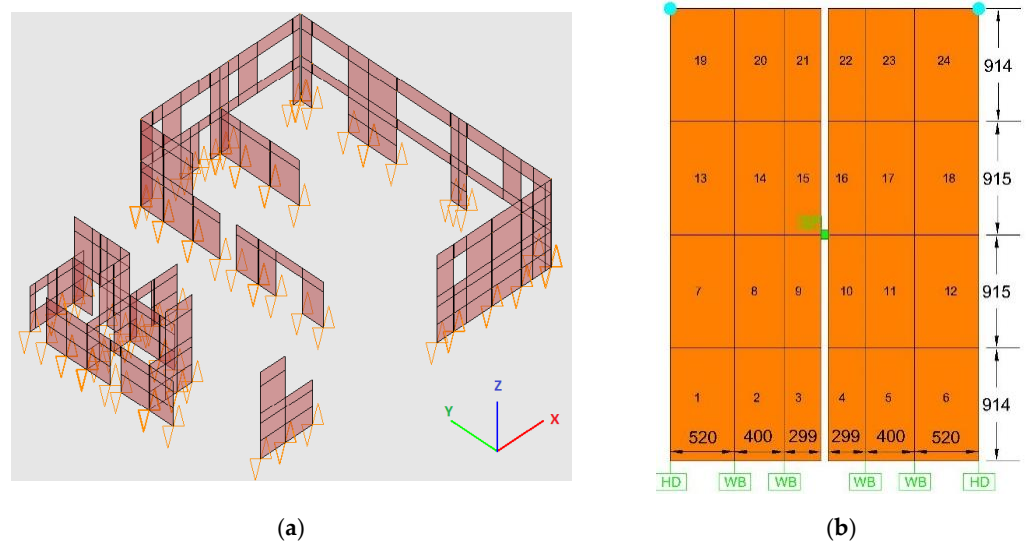


Figure 3. Numerical models: (a) case study building; (b) the balloon shear wall (unit: mm).

The energy-dissipative HDs (HD1–3) were modeled to resist tension and compression. For the tension behavior, Pinching4 material was used, whereas for the compression, an

elastic-no-tension (ENT) material model with an elastic modulus of 1500 MPa was used. Pinching4 material for HD1–3 was calibrated with test data [30]. HD4 and HD5 were modeled as elastic with stiffness in accordance with the design data of 44,270 kN/m and 73,780 kN/m, respectively. In out-of-plane direction, all HDs were defined as linear elastic, based on previous research [36].

For panel-to-panel joints, Pinching4 material was used in shear direction (Z axes) only. For other directions (X and Y axes), in-plane and out-of-plane, the joints were modeled elastically. For SP1–3 that include both nails and screws, each fastener was separately modeled and calibrated with tests [30] with a Pinching4 material and then were connected parallelly. For SP7 and SP8 that use screws only, Pinching4 materials were calibrated using test data [37]. SP11 was modeled elastically with a 60,000 kN/m stiffness based on the design. For modeling the orthogonal wall-to-wall corner connections, a rigid connection was assumed for in- and out-of-plane directions, whereas a stiffness of 60,000 kN/m was used for the Z direction.

For the WB connections, based on the number of screws along the shear walls, zero-length elements were modelled to resist tension and shear. It has been reported that conventional angle bracket connections have similar strength in tension and shear [38,39], so the same Pinching4 parameters were assigned in both directions. Since there is no test data available for WB connections, it was simplified that the elastic region of the Pinching4 material was determined using the design strength of the WB connections (3.8 kN per screw) and their post-yielding and hysteresis parameters were calibrated using TCN240 angle bracket cyclic test data.

2.3. Balloon Shear Wall Model Validation

Test results of balloon-type CLT shear walls [30] were used to validate the modeling approach. In the shear wall model (Figure 2b), two HDs were modeled on the outer ages of the shear walls calibrated with WHT740, 38–4Ø × 60 test data. Four angle brackets, two on each panel, were modeled and calibrated with angle bracket 200, 30–4Ø × 60. Moreover, a vertical connection was modeled between panels representing panel-to-panel spline connections. CLT wall panels were modeled with a thickness of 191 mm and defined as elastic isotropic material with modulus of elasticity of 9500 MPa, and Poisson's ratio of 0.01. A 20 kN/m vertical gravity load was applied at the top of the wall, the same as the test setup. A lateral load was applied at the top left corner of the wall panel. The horizontal deformations were then determined at the top-right corner of the shear wall, the same as the test. Figure 4 shows the reversed cyclic load-deformation response of balloon shear wall numerical model which well captured the hysteresis behavior of the test result.

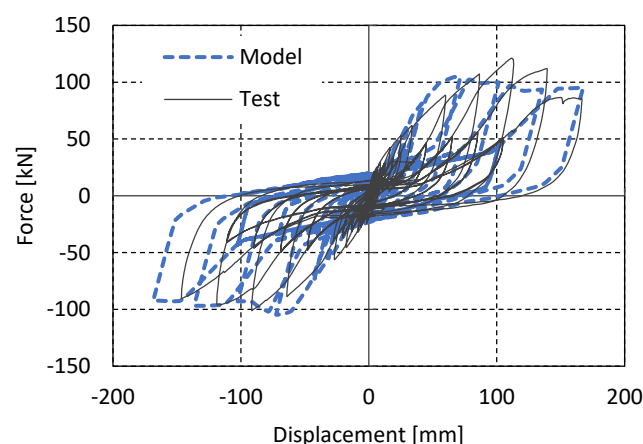


Figure 4. Shear wall model validation with test data.

2.4. Ground Motion Selection

In this study, the Zengin et al. [4] methodology was applied to isolate the duration from the amplitude, frequency content, and rate of energy build-up of the ground motion. This was achieved by selecting long and short duration record pairs that have similar spectral shapes and slopes of the Husid plot. For this purpose, first, long duration records from the S2GM [40] database were scaled and spectrally matched to a uniform hazard spectrum (UHS) for Vancouver, BC, Canada (2% probability of exceedance in 50 years) with Class C soil condition over a period range of $0.15 T$ to $1.5 s$, where T is the fundamental period of the building. Next, each long duration motion was used as a target spectrum for the PEER NGA-West2 [41] database to select a corresponding short duration record with an inherently similar response spectrum.

After constructing a subset of spectrally equivalent ground-motion pairs, the record pairs with a similar rate of energy build-up were selected. For illustration purposes, the response spectra and Husid plots of the ground motions pair #3 are compared. Both records display a similar spectral shape and amplitude over a wide period range (Figure 5a), and a similar rate of energy build-up between the two records over the significant duration (Figure 5b). The ground motion at Ciencias Agronomicas station during Maule earthquake is longer, with D_{5-95} of 38.6 s, than that from Chi-Chi (TCU053) earthquake, with D_{5-95} of 22.3 s.

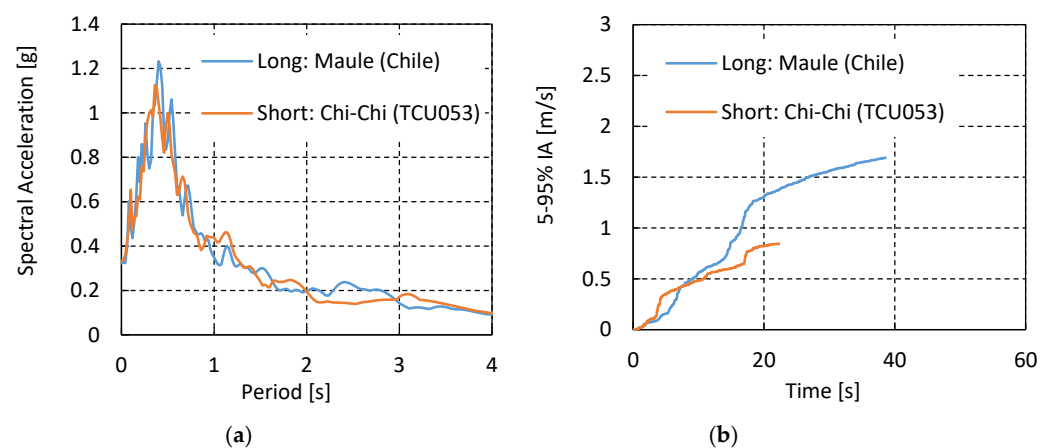


Figure 5. (a) Response spectra; (b) Husid plots of the SD and LD record pair.

Based on the recommendations of Hou and Qu [16], this study classified records with a D_{5-95} of 30 s or less as SD records, and records with D_{5-95} equal to 30 s or more as LD records. Most of the LD records were selected from subduction events, such as the 2003 and 2011 Japan earthquakes, the 1985 Mexico earthquake, and the 2010 Chile earthquake. Completing this process, a database of 24 pairs of long duration (LD) and short duration (SD) motions was generated. Appendix A presents the location, station, year, and duration of the selected ground motions. Figure 6 presents the distribution in duration among the selected ground motions. The median significant duration D_{5-95} for the LD records and the spectrally equivalent SD records are 72 s and 15 s, respectively. Figure 7 shows the response spectrum of each LD and SD motions matched to the UHS of Vancouver, BC, Canada.

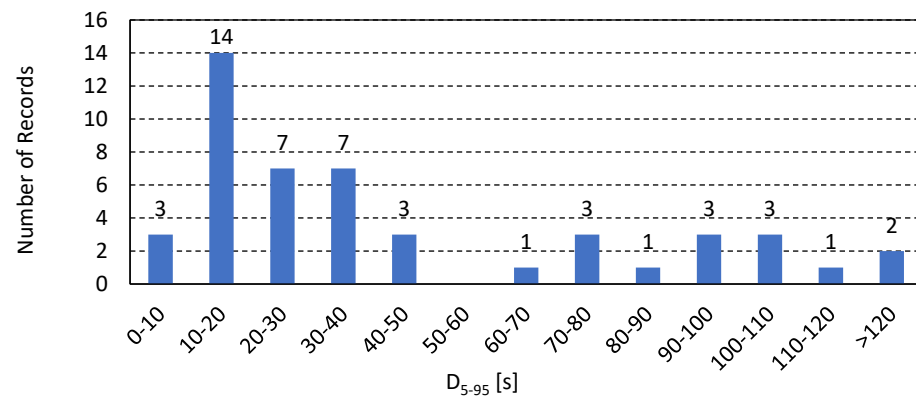


Figure 6. Distribution of D_{5-95} ground motion duration.

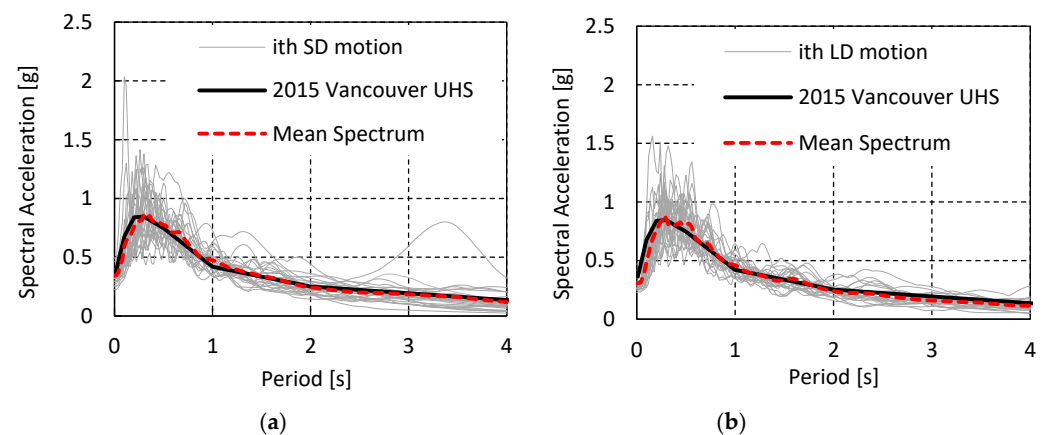


Figure 7. Response spectra of selected motions: (a) SD and (b) LD.

2.5. Analysis

Since it is impossible to have a pair of long and short duration motions that have “naturally” equivalent spectra for both horizontal components, unidirectional NLTHA was performed to evaluate the response of the building under the two sets of motions at the design intensity level in its weak long direction, as the first mode of the building model is in this direction.

Next, the effects of ground motion duration on the collapse capacity of the building were evaluated by IDA. To perform IDA, each ground motion was scaled to multiple intensity levels to approach collapse. The scaling range from 100% to 480% of UHS design intensity was used in increments of 20%. The 100% scaling level refers to the 2% in 50 year shaking level (the code design level according to the NBCC). In total, 960 NLTHA (2 sets of 24 motions at 20 intensity levels) were carried out.

Based on the IDA results, the fragility curves for the building under the two sets of motions were constructed by assuming a lognormal distribution. The cumulative probability of occurrence of damage equal to or higher than the specified drift limit was calculated using Equation (2) [42]:

$$P(C|IM = x) = \Phi\left(\frac{\ln(x/\theta)}{\beta}\right) \quad (2)$$

where $P(C|IM = x)$ is the probability that a ground motion record with intensity measure (IM) equals to x will cause the structure to collapse. $\Phi()$ is the standard normal cumulative distribution function (CDF). θ is the median of the fragility function and β is the standard deviation of $\ln IM$.

3. Results

3.1. Nonlinear Time History Analysis at Design Level

The response of the building subjected to the two sets of records was calculated using unidirectional NLTHA at design intensity level. Figure 8 shows the IDR of first (1F) and second floor (2F) of the building's long direction. The mean maximum IDR for the two record sets is close to 0.7%, which is well below the 2% drift limit specified in the 2015 NBCC for high importance buildings. The IDR of 1F under SD motions ranges from 0.51% to 1.03% with standard deviation 0.13%. However, IDR of 1F under LD motions ranges from 0.46% to 0.95% with standard deviation 0.11%. The difference in the mean maximum IDR under the two sets of motions at the design intensity level is only 0.02%. This is consistent with the results from previous studies conducted on concrete and steel frame structures [5,8,9] that duration effect on drift at design intensity level was negligible.

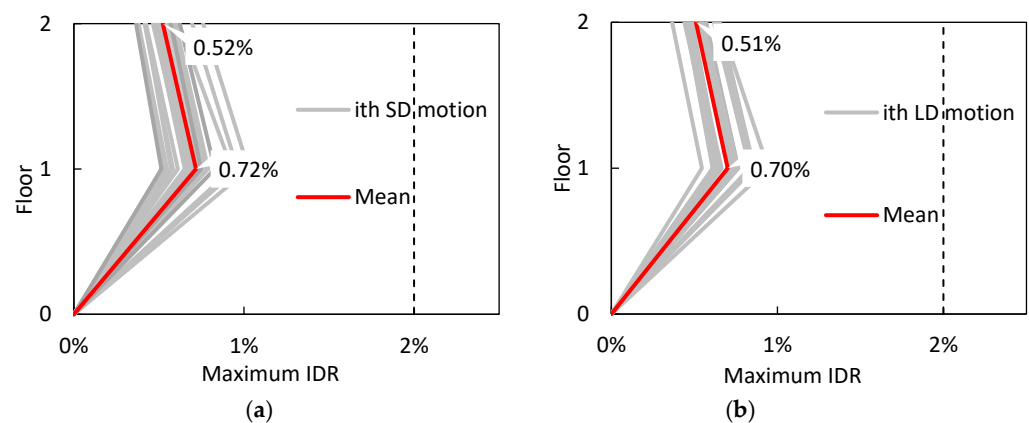


Figure 8. Maximum IDR for (a) SD and (b) LD motions.

3.2. Incremental Dynamic Analysis

It should be noted that there is no defined or observed collapse drift limit for balloon-type CLT buildings. Therefore, in this study, the collapse under each record is considered to occur when the building experiences lateral dynamic instability. The nonlinear behavior of a critical HD and WB under all the records at collapse and before collapse were evaluated. Figure 9 shows exemplarily the nonlinear behavior of a critical HD and WB under a SD (Imperial Valley-06-Brawley Airport) and a LD (Tohoku-Japan at Koga station) record (red highlighted circles in Figure 9) before collapse. These results show the critical connections performed at onset of collapse (black dots in Figure 10); however, at the next intensity level, they failed, resulting in building lateral dynamic instability.

Figure 10 illustrated the IDA curves for the building model subjected to long and short duration motions, at different intensity levels in the weak direction. Each black dot on the curve represents the onset of collapse, which means the building will collapse at the next intensity level. At the design intensity level (100% of UHS), the maximum IDRs were less than 1% under both sets of ground motions. However, with the increase of intensity, the influence of duration was observed. The IDA curves indicated that the estimated IDR for SD motions ranges from 2.2% to 9.7% whereas the IDR for LD motions ranges from 0.9% to 6.5%. Moreover, the SD motions reach an average maximum IDR of 4.8% before causing collapse. In contrast, the LD motions reach an average maximum IDR of 3.6% before collapse. This shows that LD motions are more likely to cause overall instability which will lead to collapse of the building. This finding is in agreement with recent studies on a steel moment frame [14] and light-frame wood buildings [12,13].

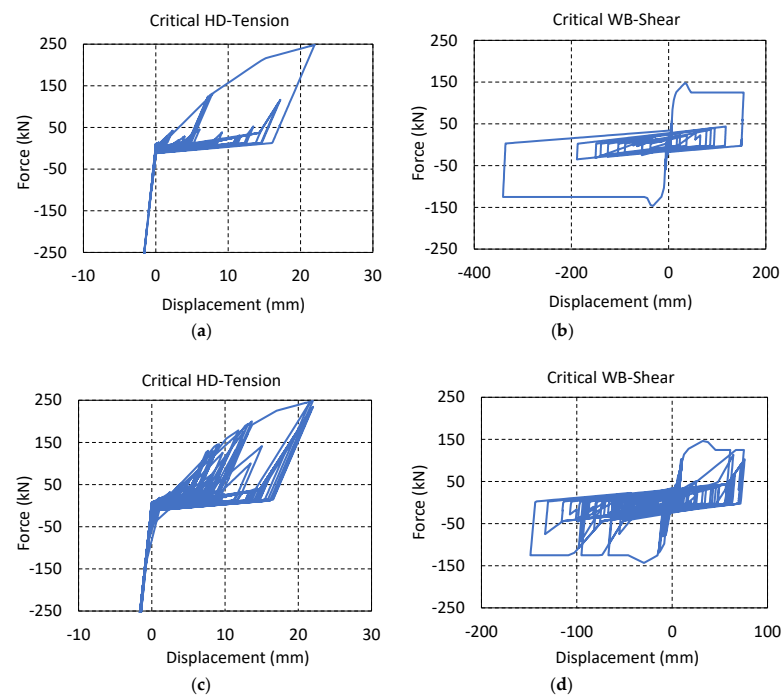


Figure 9. Nonlinear behavior of a critical (a,b) HD and WB connection under the SD record; (c,d) HD and WB connection under the LD record before collapse.

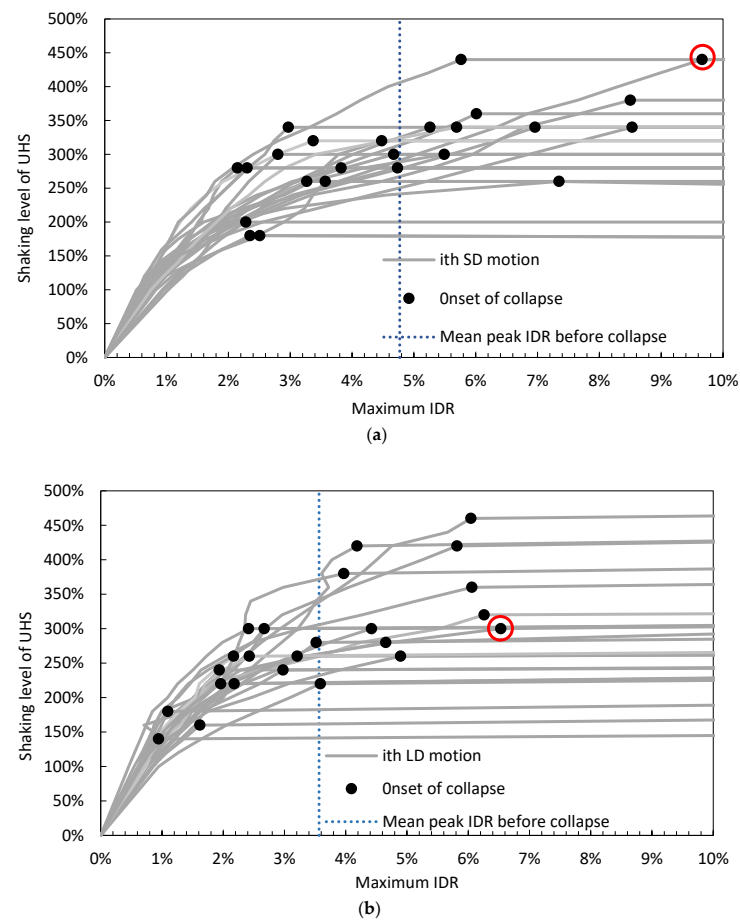


Figure 10. IDA curves of (a) SD and (b) LD motions.

3.3. Fragility Assessment

To calculate the collapse risk of the building, collapse fragility curves were derived from the IDA. Figure 11a,b show the fragility curves for the two sets of motions. In this figure, the black dots refer to the empirical collapse data points and the red line is the CDF by fitting a lognormal distribution through these empirical points. The building had 0% probability of collapse at the design intensity level under the two sets of motions. However, with increasing intensity, the building starts to exhibit a higher probability of collapse under LD motions. The median collapse capacity (50% probability of collapse) for LD motions was determined at 292% of UHS intensity level. In contrast, the median collapse capacity for SD motions was determined at 318% of UHS, a reduction in the median collapse capacity of 9%. These results show that ground motion duration affects the collapse risk for CLT buildings. The conclusion that ground motion duration reduces the median collapse scaling level of structures is consistent with the findings for steel or concrete moment-resisting frames and on wood frame buildings [4,8–13].

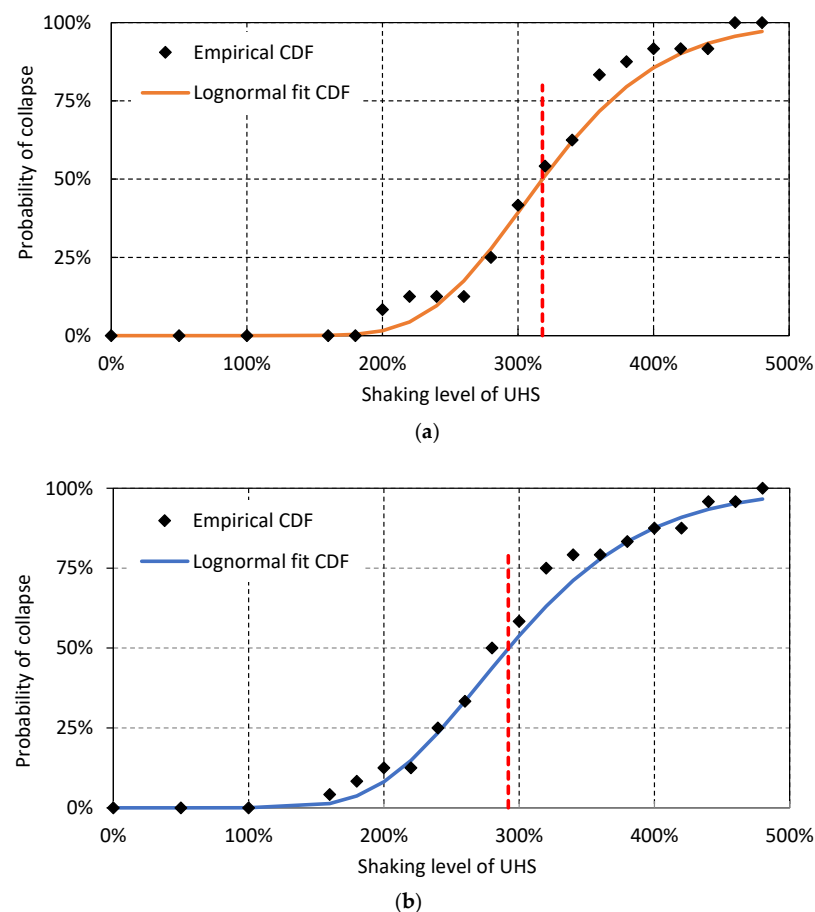


Figure 11. Fragility curves for collapse. (a) SD; (b) LD motions.

4. Discussion and Conclusions

The effects of ground motion duration on a newly constructed two-storey balloon-type CLT building, designed for Vancouver, BC, Canada, were evaluated. Test results were used to validate an OpenSees model with calibrated connector properties. A database including 24 pairs of long and short duration records with similar amplitude, frequency content, and the rate of energy build-up was established to isolate the duration from other ground motion characteristics. NLTHA and IDA were conducted to investigate the seismic response of the building, and fragility curves were developed to assess the collapse capacity.

The following conclusions can be drawn: (1) At design intensity level, ground motion duration was found not critical since the difference in inter-storey drift ratio between the

two sets of records was negligible; (2) however, at higher intensity levels, LD motions increased the building's probability of collapse. The average maximum IDR before collapse for LD and SD motions were 3.6% and 4.8%, respectively, meaning that LD events are more likely to cause structural collapse; and (3) LD motions reduced the median collapse capacity of the building by 9% as a result of the greater number of inelastic cycles.

This is the first study that evaluated the effect of duration on the seismic performance of a CLT building, and only the second study using the methodology presented by Zengin et al. [4], where the initial rate of Arias Intensity is used as a control parameter in addition to amplitude and frequency content in ground motion selection. The results are based on a high importance category building with a very conservative design (0.72% maximum IDR). Thus, further research is required to evaluate the duration effects on the seismic performance of normal importance category, taller and platform-type CLT buildings.

Author Contributions: Formal analysis, investigation, writing—original draft, M.J.; data curation, validation, methodology, validation, writing—review and editing, Y.P.; conceptualization, validation, writing—review and editing, M.S.; funding acquisition, methodology, supervision, writing—review and editing, T.T. All authors have read and agreed to the published version of the manuscript.

Funding: This research was funded by Natural Resources Canada (NRCAN) through the Green Construction Wood (GCWood) program, and by the Government of Canada through a Canada Research Chair.

Data Availability Statement: The data presented from the UNBC research are available on request from the corresponding author.

Acknowledgments: The project was supported by Fast + Epp.

Conflicts of Interest: The authors declare no conflict of interest.

Appendix A. Selected Ground Motions

Long Duration Subduction Motions				Short Duration Crustal Motions			
Event	Year	Station	D_{5-95} [s]	Event	Year	Station	D_{5-95} [s]
Hokkaido (Japan)	2003	Horokeshi	32.9	Chi-Chi	1999	TCU054	24.5
Tohoku (Japan)	2011	Hiratsuka-st5	118.1	Chi-Chi	1999	TCU029	23.6
Maule (Chile)	2010	Ciencias Agr.	38.6	Chi-Chi	1999	TCU053	22.3
Hokkaido (Japan)	2003	Urakawa	39.2	Loma Prieta	1989	Hollister Diff. Array	12.4
Tohoku (Japan)	2011	Hachiohji	75.0	Chi-Chi	1999	CHY035	13.2
Tohoku (Japan)	2011	Takasaki	71.6	Manjil	1990	Abhar	21.1
Hokkaido (Japan)	2003	Akan	35.7	Kalamata, Greece-01	1986	Kalamata	5.0
Tohoku (Japan)	2011	Okudo	108.9	Taiwan Smart-01	1986	SMART1-I01	20.4
Tohoku (Japan)	2011	Koganei	67.8	Taiwan Smart-01	1986	SMART1-O02	16.3
Tohoku (Japan)	2011	Shinozaki	107.7	Taiwan Smart-01	1986	SMART1-I02	21.6
Tohoku (Japan)	2011	Nakoso	88.1	Imperial Valley-06	1979	El Centro Array #3	11.9
Maule (Chile)	2010	Santiago Center	35.2	Imperial Valley-06	1979	Brawley Airport	14.1
Maule (Chile)	2010	Colegio Las Am.	37.1	Taiwan Smart-01	1986	SMART1-E01	8.7
Maule (Chile)	2010	La Florida	39.9	Chi-Chi	1999	TCU051	24.2
Tohoku (Japan)	2011	Gyoutoku	102.0	Loma Prieta	1989	Oakland-Outer Harbor	8.7
Tohoku (Japan)	2011	Nishiaidu	90.9	Imperial Valley-06	1979	Holtville Post Office	11.8
Tohoku (Japan)	2011	Chiba	93.5	Superstition Hills-02	1987	Kornbloom Road	14.0
Michoacan (Mexico)	1985	Villita	44.1	Loma Prieta	1989	Palo Alto-SLAC Lab	11.6
Hokkaido (Japan)	2003	Hobetsu	40.9	Superstition Hills-02	1987	Poe Road	13.6
Hokkaido (Japan)	2003	Oiwake	44.6	Northridge-01	1994	Santa Monica City Hall	10.7
Tohoku (Japan)	2011	Koga	93.9	Loma Prieta	1989	Anderson Dam (L Abut)	12.7
Tohoku (Japan)	2011	Hiratsuka-st1	127.6	Chi-Chi	1999	CHY028	12.1
Tohoku (Japan)	2011	Kawagoe	73.4	Imperial Valley-06	1979	El Centro Array #1	15.0
Tohoku (Japan)	2011	Tatsumi	120.1	Imperial Valley-06	1979	EC County Center FF	10.4

References

- Clague, J.J. Evidence for large earthquakes at the Cascadia subduction zone. *Rev. Geophys.* **1997**, *35*, 439–460. [\[CrossRef\]](#)
- Atwater, B.F.; Hemphill-Haley, E. *Recurrence Intervals for Great Earthquakes of the Past 3500 Years at Northeastern Willapa Bay, Washington*; US Government Printing Office: Washington, DC, USA, 1997.
- Foschaar, J.; Baker, J.; Deierlein, G. Preliminary assessment of ground motion duration effects on structural collapse. In Proceedings of the 15th World Conference on Earthquake Engineering, Lisbon, Portugal, 24–28 September 2012.
- Zengin, E.; Abrahamson, N.A.; Kunnath, S. Isolating the effect of ground-motion duration on structural damage and collapse of steel frame buildings. *Earthq. Spectra* **2020**, *36*, 718–740. [\[CrossRef\]](#)
- Barbosa, A.R.; Ribeiro, F.L.; Neves, L.A. Influence of earthquake ground-motion duration on damage estimation: Application to steel moment resisting frames. *Earthq. Eng. Struct. Dyn.* **2017**, *46*, 27–49. [\[CrossRef\]](#)
- Kiani, J.; Camp, C.; Pezeshk, S. Role of conditioning intensity measure in the influence of ground motion duration on the structural response. *Soil Dyn. Earthq. Eng.* **2018**, *104*, 408–417. [\[CrossRef\]](#)
- Marsh, M.; Gianotti, C. *Structural Response to Long-Duration Earthquakes*; Final Report; Washington State Department of Transportation: Olympia, WA, USA, 1994.
- Raghunandan, M.; Liel, A.B. Effect of ground motion duration on earthquake-induced structural collapse. *Struct. Saf.* **2013**, *41*, 119–133. [\[CrossRef\]](#)
- Han, J.; Sun, X.; Zhou, Y. Duration effect of spectrally matched ground motion records on collapse resistance capacity evaluation of RC frame structures. *Struct. Des. Tall Spec. Build.* **2017**, *26*, e1397. [\[CrossRef\]](#)
- Fairhurst, M.; Bebamzadeh, A.; Ventura, C.E. Effect of ground motion duration on reinforced concrete shear wall buildings. *Earthq. Spectra* **2019**, *35*, 311–331. [\[CrossRef\]](#)
- Pan, Y.; Ventura, C.E.; Tannert, T. Damage index fragility assessment of low-rise light-frame wood buildings under long duration subduction earthquakes. *Struct. Saf.* **2020**, *84*, 101940. [\[CrossRef\]](#)
- Pan, Y.; Ventura, C.E.; Finn, W.L. Effects of ground motion duration on the seismic performance and collapse rate of light-frame wood houses. *J. Struct. Eng.* **2018**, *144*, 04018112. [\[CrossRef\]](#)
- Pan, Y.; Ventura, C.E.; Finn, W.L.; Xiong, H. Effects of ground motion duration on the seismic damage to and collapse capacity of a mid-rise woodframe building. *Eng. Struct.* **2019**, *197*, 109451. [\[CrossRef\]](#)
- Chandramohan, R.; Baker, J.W.; Deierlein, G.G. Quantifying the influence of ground motion duration on structural collapse capacity using spectrally equivalent records. *Earthq. Spectra* **2016**, *32*, 927–950. [\[CrossRef\]](#)
- Hou, H.; Qu, B. Duration effect of spectrally matched ground motions on seismic demands of elastic perfectly plastic SDOFS. *Eng. Struct.* **2015**, *90*, 48–60. [\[CrossRef\]](#)
- Trifunac, M.D. Power design method. In Proceedings of the Earthquake Engineering in the 21st Century to Mark 40th Anniversary of IZS-Skopje, Skopje, Macedonia, 28 August–1 September 2005.
- Husid, R. Características de terremotos. Análisis general. *Rev. IDIEM* **1969**, *8*, 21–42.
- Bommer, J.J.; Martinez-Pereira, A. The effective duration of earthquake strong motion. *J. Earthq. Eng.* **1999**, *3*, 127–172. [\[CrossRef\]](#)
- Trifunac, M.D.; Brady, A.G. A study on the duration of strong earthquake ground motion. *Bull. Seismol. Soc. Am.* **1975**, *65*, 581–626.
- Arias, A. *A Measure of Earthquake Intensity in Seismic Design of Nuclear Power Plants*; Hansen, R.J., Ed.; Institute of Technology Press: Cambridge, MA, USA, 1970.
- Shahnewaz, M.D.; Alam, M.S.; Tannert, T. In-plane Strength and Stiffness of Cross-laminated Timber Shear Walls. *Buildings* **2018**, *8*, 100. [\[CrossRef\]](#)
- Tannert, T.; Follesa, M.; Fragiocomo, M.; González, P.; Isoda, H.; Moroder, D.; Xiong, H.; van de Lindt, J.W. Seismic Design of CLT Buildings. *Wood Fiber. Sci.* **2018**, *50*, 3–26. [\[CrossRef\]](#)
- Izzi, M.; Casagrande, D.; Bezzi, S.; Pasca, D.; Follesa, M.; Tomasi, R. Seismic behaviour of Cross-Laminated Timber structures: A state-of-the-art review. *Eng. Struct.* **2018**, *170*, 42–52. [\[CrossRef\]](#)
- Tannert, T.; Loss, C. Contemporary and Novel Hold-Down Solutions for Mass Timber Shear Walls. *Buildings* **2022**, *12*, 202. [\[CrossRef\]](#)
- NBCC (National Building Code of Canada). *Canadian Commission on Building and Fire Codes*; National Research Council of Canada: Ottawa, ON, Canada, 2020.
- CSA Standard O86-19; Canadian Standards Association (CSA), Engineering Design in Wood. CSA: Toronto, ON, Canada, 2019.
- Sustersic, I.; Fragiocomo, M.; Dujic, B. Seismic analysis of cross-laminated multistory timber buildings using code-prescribed methods: Influence of panel size, connection ductility, and schematization. *J. Struct. Eng.* **2016**, *142*, E4015012. [\[CrossRef\]](#)
- Amini, M.O.; van de Lindt, J.W.; Rammer, D.; Pei, S.; Line, P.; Popovski, M. Systematic experimental investigation to support the development of seismic performance factors for cross laminated timber shear wall systems. *Eng. Struct.* **2018**, *172*, 392–404. [\[CrossRef\]](#)
- Ceccotti, A.; Sandhaas, C.; Okabe, M.; Yasumura, M.; Minowa, C.; Kawai, N. SOFIE project-3D shaking table test on a seven-storey full-scale cross-laminated timber building. *Earthq. Eng. Struct. Dyn.* **2013**, *42*, 2003–2021. [\[CrossRef\]](#)
- Shahnewaz, M.; Dickof, C.; Tannert, T. Seismic Behavior of Balloon Frame CLT Shear Walls with Different Ledgers. *J. Struct. Eng.* **2021**, *147*, 04021137. [\[CrossRef\]](#)

31. Zhang, X.; Pan, Y.; Tannert, T. The influence of connection stiffness on the dynamic properties and seismic performance of tall cross-laminated timber buildings. *Eng. Struct.* **2021**, *238*, 112261. [[CrossRef](#)]
32. Shahnewaz, M.; Pan, Y.; Shahria Alam, M.; Tannert, T. Seismic Fragility Estimates for Cross-Laminated Timber Platform Building. *J. Struct. Eng.* **2020**, *146*, 04020256. [[CrossRef](#)]
33. Sun, X.; He, M.; Li, Z.; Shu, Z. Performance evaluation of multi-storey cross-laminated timber structures under different earthquake hazard levels. *J. Wood Sci.* **2018**, *64*, 23–39. [[CrossRef](#)]
34. Mazzoni, S.; McKenna, F.; Scott, M.H.; Fenves, G.L. *OpenSees Command Language Manual*; Pacific Earthquake Engineering Research (PEER) Center: Berkeley, CA, USA, 2006; Volume 264, pp. 137–158.
35. Lowes, L.N.; Mitra, N.; Altoontash, A. *A Beam-Column Joint Model for Simulating the Earthquake Response of Reinforced Concrete Frames*; Report; Pacific Earthquake Engineering Research (PEER) Center: Berkeley, CA, USA, 2003.
36. Sullivan, K.; Miller, T.H.; Gupta, R. Behavior of cross-laminated timber diaphragm connections with self-tapping screws. *Eng. Struct.* **2018**, *168*, 505–524. [[CrossRef](#)]
37. Gavric, I.; Fragiocomo, M.; Ceccotti, A. Cyclic behavior of typical screwed connections for cross-laminated (CLT) structures. *Eur. J. Wood Wood Prod.* **2015**, *73*, 179–191. [[CrossRef](#)]
38. Tomasi, R.; Smith, I. Experimental characterization of monotonic and cyclic loading responses of CLT panel-to-foundation angle bracket connections. *J. Mater. Civ. Eng.* **2015**, *27*, 04014189. [[CrossRef](#)]
39. Masroor, M.; Doudak, G.; Casagrande, D. The effect of bi-axial behaviour of mechanical anchors on the lateral response of multi-panel CLT shearwalls. *Eng. Struct.* **2020**, *224*, 111202. [[CrossRef](#)]
40. S2GM, Selection and Scaling Ground Motions (S2GM). Available online: <http://s2gm.hpcperformance.design.com/login.php?e=1> (accessed on 15 November 2021).
41. PEER, Pacific Earthquake Engineering Research (PEER) NGA-West2 Database. Berkeley, CA. Available online: <https://ngawest2.berkeley.edu/> (accessed on 15 November 2021).
42. Baker, J.W. Efficient analytical fragility function fitting using dynamic structural analysis. *Earthq. Spectra* **2015**, *31*, 579–599. [[CrossRef](#)]